Improving *H*-mode Pedestal Temperature Scalings with Second Ballooning Stability

Thawatchai Onjun
Plasma and Fusion Research Unit, Sirindhorn International Institute of Technology,
Thammasat University, Pathum Thani, 12121, Thailand

Abstract

Models for predicting pedestal ion temperature and pedestal electron density at the edge of type I ELMy *H*-mode plasmas are developed. Both parameters are important parameters for improved performance in burning plasma experiments. The pedestal temperature models are developed based on theoretically motivated concepts for both pedestal width and pedestal pressure gradient. In this work, the pedestal pressure gradient is assumed to be controlled by a ballooning mode limit, in which the effects of both first and second stability limits are considered. The edge bootstrap current, which results from a strong edge pressure gradient near the plasma edge, can reduce the magnetic shear so that plasma can make a transition from the first stability regime of ballooning mode to the second stability regime of ballooning mode, which results in higher edge pressure gradient and, consequently, higher pedestal temperature. The magnetic shear and safety factor used in the pedestal calculation are at the top of the pedestal. The predictions of each pedestal models are compared with pedestal data for type I ELMy *H*-mode discharges obtained from the latest public version (version 3.2) in the International Tokamak Physics Activity Edge (ITPA) Pedestal Database. It is found that the inclusion of the second ballooning stability effect can improve the predictive capability of the model based on the magnetic and flow shear stabilization (RMSE of 28.2%). For the pedestal density, it is developed using an empirical approach. It is found that the best model, which is a function of plasma engineering parameters including line average density, plasma current and toroidal magnetic field, yields an agreement of 10.9% RMSE when its predictions are compared against experimental data. Both pedestal temperature and density models are used to predict the pedestal parameters for the standard type I ELMy *H*-mode scenario of ITER, predictive analysis yields ion temperatures at the top of the *H*-mode pedestal in the range from 1.7 to 1.9 keV.

Keywords: Plasma, Tokamak, Fusion, *H*-mode, Pedestal, Stability, ITER

1. Introduction

It is widely known that plasmas can undergo a spontaneous self-organizing transition from a low confinement mode (*L*-mode) to a high confinement mode (*H*-mode) when sufficient plasma heating power is applied. This transition results in a suppression of edge turbulence, which yields better energy confinement in the *H*-mode plasma [1]. The energy confinement in the *H*-mode regime of tokamaks strongly depends on the plasma parameters at the top of the pedestal that forms at the edge of *H*-mode plasmas. The *H*-mode temperature and density pedestal is produced by a

transport barrier characterized by a narrow sharply defined region of steep temperature and density gradients. This pedestal is located near the last closed magnetic flux surface and typically extends over with a width of less than 5% – 10% of the plasma minor radius. Since the height of the pedestal strongly influences the plasma performance in the *H*-mode operation, it is important to understand the physics that governs the *H*-mode pedestal, which is an important issue for burning plasma experiments such as the International Thermonuclear Experimental Reactor (ITER) [2].

In the previous pedestal study by T. Onjun *et al*. [3], six theory-based pedestal temperature models were developed using different models for the pedestal width together with a ballooning mode pressure gradient limit that is restricted to the first stability of ballooning modes. These models also include the effects of geometry, bootstrap current, and separatrix, leading to a complicated nonlinear behavior. For the best model, the agreement between the model's predictions and experimental data for pedestal temperature is about 30.8% RMSE for 533 data points from the International Tokamak Physics Activity Edge (ITPA) Pedestal Database. One weakness of these pedestal temperature models is the assumption that the plasma pedestal is in the first stability regime of ballooning modes.

In this study, six pedestal ion temperature models [3] based on six different pedestal width scalings [3-8] are modified to include the effect of the second stability limit of ballooning modes. It is widely accepted that plasma can gain access to second stability, which results in significant improvement of the pedestal pressure gradient and, consequently, pedestal pressure [9-11]. The predictions from these pedestal temperature models are tested against the latest public version of the pedestal data (Version 3.2) obtained from the ITPA Pedestal Database. This paper is organized in the following way: In Section 2, the pedestal temperature model development is described. In Section 3, the experimental data used, is described. In section 4, the predictions of the pedestal ion temperature resulting from the models are compared with pedestal ion temperature experimental data. A simple statistical analysis is used to characterize the agreement of the predictions of each pedestal model with experimental data. In addition, the development and comparison with experimental data for the pedestal density models and the prediction of the pedestal in ITER is shown. In Section 6, conclusions are presented.

2. *H*-Mode Pedestal Temperature

A simple picture of the pedestal region in *H*-mode plasma can be illustrated in Fig. 1. If the pressure gradient ($\partial p/\partial r$) within the pedestal region is assumed to be constant, the plasma pressure at the top of pedestal (p_{ped}) can be estimated in terms of density and temperature at the top of the pedestal as:

$$p_{\text{ped}} = 2n_{\text{ped}}kT_{\text{ped}} = \Delta\left|\frac{\partial p}{\partial r}\right| \qquad (1)$$

where n_{ped} and T_{ped} are the density and temperature at the top of the pedestal, k is the Boltzmann's constant, and Δ is the pedestal width. Rewriting Eq. (1), the temperature at the top of the pedestal can be estimated as:

$$T_{\text{ped}} = \frac{1}{2n_{\text{ped}}k}\left|\frac{\partial p}{\partial r}\right|\Delta \qquad (2)$$

In determining the pressure gradient inside the pedestal region for the type I ELMy *H*-mode discharges, it is assumed that the pressure gradient is limited by the ballooning mode instability [12]. Recognizing that the pressure gradient in the pedestal region may depend on parameters such as magnetic shear (s), elongation (κ), and triangularity (δ), we define the

maximum normalized pressure gradient, that is the critical pressure gradient, α_c, as:

$$\alpha_c \equiv -\frac{2\mu_0 Rq^2}{B_T^2}\frac{\partial p}{\partial r} = \alpha_c(s,\kappa,\delta) \qquad (3)$$

Note that definitions of the variables used in this paper are given in Table 1. The temperature at the top of pedestal can then be computed in terms of α_c using the equation:

$$T_{ped} = \frac{\Delta}{2n_{ped}k}\frac{\alpha_c B_T^2}{2\mu_0 Rq^2} \qquad (4)$$

If the maximum normalized pressure gradient and the pedestal width are determined, Eq. (4) can be used to obtain the temperature at the top of the pedestal.

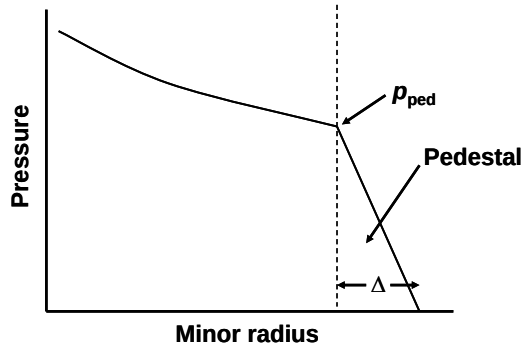

Figure 1: Plot for the pressure profile near the edge of the H-mode plasmas. The H-mode edge pedestal is a region of steep gradient at the edge of plasma.

It is worth noting that in this paper, we consider the time average of the pedestal temperature. Consequently, the time-dependent effects of ELMs are not considered. The plasma ions are assumed to be primarily hydrogenic. The only effect of the impurity concentration is through the calculation of the plasma collisionality, which affects the bootstrap current. Also, it is assumed that the electron and ion temperatures are equal.

2.1 Pedestal Width

In this study, six theory-motivated models for the pedestal width are used to determine scalings for the pedestal ion temperatures that are compared with experimental data.

2.1.1 Magnetic and Flow Shear Stabilization Width Scaling

The basic assumption of this model is that the transport barrier is formed in the region, where the turbulence growth rate is balanced, by a stabilizing E_rxB shearing rate [4]. The scaling of the pedestal width is found to be:

$$\Delta = C_{w,1}\rho_i s^2 = C_{w,1}\left(\frac{4.57\times10^{-3}\sqrt{A_H T_{ped}}}{B_T}\right)s^2 \qquad (5)$$

where A_H is the average hydrogenic mass. By using this scaling for the pedestal width in Eq. (3), the temperature at the top of pedestal can be obtained from:

$$T_{ped} = C_{w,1}^2\left(\frac{4.57\times10^{-3}}{2.82\mu_0\left(1.6022\times10^{-16}\right)}\right)^2\left(\frac{B_T}{q}\right)^2\left(\frac{\sqrt{A_H}}{R}\right)^2\left(\frac{\alpha_c}{n_i}\right)^2 \qquad (6)$$

where $C_{w,1}$ is the constant of proportionality in Eq. (5).

2.1.2 Flow Shear Stabilization Width Scaling

In this model, the E_rxB suppression of long wavelength modes is assumed to be the relevant factor in establishing the edge transport barrier [3]. The following result for the pedestal width is obtained:

$$\Delta = C_{w,2}\sqrt{\rho_i Rq} \qquad (7)$$

By combining Eqs. (4) and (7), the temperature at the top of the pedestal can be obtained from the non-linear equation (which again contains T_{ped}) on both left and right sides):

$$T_{ped} = C_{w,2}^{4/3}\left(\frac{4.57\times10^{-3}}{2.82\mu_0\left(1.6022\times10^{-16}\right)}\right)^{4/3}\left(\frac{B_T}{q}\right)^2\left(\frac{\sqrt{A_H}}{R}\right)^{2/3}\left(\frac{\alpha_c}{n_i}\right)^{4/3} \qquad (8)$$

where $C_{w,2}$ is the constant of proportionality in Eq. (7).

2.1.3 Normalized Poloidal Pressure Width Scaling

In this model, the scaling of pedestal width is based on a model proposed by T. Osborne [5].

$$\Delta = C_{\mathrm{w},3}\sqrt{\beta_{\theta,ped}}R = C_{\mathrm{w},3}\sqrt{\frac{4\mu_0 n_{\mathrm{ped}} kT_{\mathrm{ped}}}{\langle B_\theta\rangle^2}}R \qquad (9)$$

where β_θ is the normalized poloidal pressure and $\langle B_\theta\rangle$ is the average poloidal field around the flux surface. By using Eq. (4) and Eq. (9), the temperature at the top of pedestal can be obtained from the equation:

$$T_{\mathrm{ped}} = C_{\mathrm{w},3}^2\left(\frac{1}{2.82\mu_0\left(1.6022\times10^{-16}\right)}\right)\left(\frac{B_{\mathrm{T}}}{q^2}\right)^2\left(\frac{R}{a}\right)^2\left(\frac{\alpha_c^2}{n_{\mathrm{i}}}\right)\left(\frac{\pi q_{95}\left(1+\kappa_{95}\right)}{5g_s}\right)^2 \qquad (10)$$

where $C_{\mathrm{w},3}$ is the constant of proportionality in Eq. (9) and q_{95}, the safety factor at the 95% flux surface, with geometrical effects included, is defined by:

$$q_{95} = \frac{5a^2 B_{\mathrm{T}}}{\mu_0 I_{\mathrm{p}} R} g_{\mathrm{s}}\left(\varepsilon,\kappa_{95},\delta_{95}\right) \qquad (11)$$

and where the geometrical factor, g_s, is taken to be:

$$g_s\left(\varepsilon,\kappa_{95},\delta_{95}\right) = \frac{\left(1+\kappa_{95}^2\left(1+2\delta_{95}^2-1.2\delta_{95}^3\right)\right)\left(1.17-0.65\varepsilon\right)}{2\left(1-\varepsilon^2\right)^2} \qquad (12)$$

which is similar to Uckan's approximate fit [13] to numerical equilibria expressing the safety factor q_{95} in terms of the magnetic field, plasma current, and shaping effects such as elongation κ_{95}, triangularity δ_{95} (assumed to be approximately 0.85 times the value of triangularity at the separatrix), and inverse aspect ratio $\varepsilon = a/R$.

2.1.4 2D Fluid Equilibria Width Scaling

In this model, the scaling of pedestal width is based on the double-Beltrami two-fluid equilibria of Mahajan and Yoshida [6]. It is found that the scaling for the pedestal width is:

$$\Delta = C_{\mathrm{w},4}\frac{0.023}{Z}\sqrt{\frac{A_H}{n_{\mathrm{ped},20}}} \qquad (13)$$

where Z is the ion charge, $n_{\mathrm{ped},20}$ is the pedestal density in the unit of 10^{20} particles/m^3. Note that in Ref. [6], $C_{\mathrm{w},4}$ is taken to be 1. In this work, $C_{\mathrm{w},4}$ is taken to be 1 or a constant chosen to optimize agreement with experimental data. By using Eq. (4) and Eq. (13), the temperature at the top of pedestal can be obtained from the non-linear equation:

$$T_{\mathrm{ped}} = C_{\mathrm{w},4}\left(\frac{0.023\times10^{10}}{4\left(0.71\right)^{3/2}\mu_0\left(1.6022\times10^{-16}\right)}\right)\left(\frac{B_{\mathrm{T}}}{q}\right)^2\left(\frac{\sqrt{A_H}}{RZ}\right)\left(\frac{\alpha_c}{n_{\mathrm{i}}^{3/2}}\right) \qquad (14)$$

where $C_{\mathrm{w},4}$ is the constant of proportionality in Eq. (13).

2.1.5 Diamagnetic Stabilization Width Scaling

In this model, the scaling of pedestal width is based on a model proposed by B. Rogers [7].

$$\Delta = \boldsymbol{C}_{\mathrm{W},5}\boldsymbol{\rho}^{2/3}\boldsymbol{R}^{1/3} \qquad (15)$$

By combining Eqs. (4) and (15), the temperature at the top of the pedestal can be obtained from the non-linear equation (which again contains T_{ped}) on both left and right sides):

$$\boldsymbol{T}_{ped} = \boldsymbol{C}_{\mathrm{W},5}^{3/2}\left(\left(\frac{\left(4.57\times10^{-3}\right)^{2/3}}{4\boldsymbol{\mu}_0\left(1.6022\times10^{-16}\right)}\right)^{3/2}\left(\frac{\boldsymbol{B}_T^2}{\boldsymbol{q}^3}\right)\left(\frac{\sqrt{\boldsymbol{A}_H}}{\boldsymbol{R}}\right)\left(\frac{\boldsymbol{\alpha}_c}{\boldsymbol{n}_{ped}}\right)^{3/2}\right) \qquad (16)$$

where $C_{\mathrm{w},5}$ is the constant of proportionality in Eq. (15).

2.1.6 Ion Orbit Loss Width Scaling

In this model, the scaling of pedestal width is based on a model proposed by K. C. Shaing [8].

$$\Delta = \boldsymbol{C}_{\mathrm{W},6}\sqrt{\boldsymbol{\varepsilon}}\boldsymbol{\rho} \qquad (17)$$

By combining Eqs. (4) and (17), the temperature at the top of the pedestal can be obtained from the non-linear equation (which again contains T_{ped}) on both left and right sides):

$$\boldsymbol{T}_{ped} = \boldsymbol{C}_{\mathrm{W},6}^2\left(\left(\frac{\left(4.57\times10^{-3}\right)^{2/3}}{4\boldsymbol{\mu}_0\left(1.6022\times10^{-16}\right)}\right)^2\left(\frac{\boldsymbol{B}_T}{\boldsymbol{q}}\right)^2\left(\frac{\boldsymbol{A}_H}{\boldsymbol{\kappa}_{95}^2\boldsymbol{aR}}\right)\left(\frac{\boldsymbol{\alpha}_c}{\boldsymbol{n}_{ped}}\right)^2\right) \qquad (18)$$

where $C_{\mathrm{w},6}$ is the constant of proportionality in Eq. (17).

2.2 Pedestal Pressure Gradient

For the maximum pressure gradient in the pedestal of type I ELMy *H*-mode discharges, the pedestal pressure gradient is approximated as the pressure gradient limits of high-*n* ballooning modes in the short

toroidal wavelength limit. The ballooning mode is usually described using the magnetic shear vs. normalized pressure gradient diagram (*s*-α diagram). Normally, the calculation of ballooning mode stability is complicated, requiring information about the plasma equilibrium and geometry. A number of different codes have been developed for stability analysis, such as MISHKA and ELITE. In Ref. [14], stability analyses for JET triangularity scan *H*-mode discharges were carried out using the HELENA and MISHKA ideal MHD stability codes. For the JET high triangularity discharge 53298, the stability analysis results are shown in Figure 10 of that reference. Based on that result, the *s*-α MHD stability diagram, where both first and second stability effects are included, can be simplified as Fig. 2. This *s*-α MHD stability diagram leads to an analytic expression for α_c that includes the effect of both first and second stability of ballooning modes and geometrical effects given by:

$$\alpha_c = \alpha_0(s)\left(\frac{1+\kappa_{95}^2\left(1+10\delta_{95}^2\right)}{7}\right) \qquad (19)$$

where *s* is the magnetic shear, κ_{95} and δ_{95} are the elongation and triangularity at the 95% flux surface, and $\alpha_0(_s)$ is a function of magnetic shear :

$$\alpha_0(s) = \begin{cases} 3+0.8(s-4) & ; s > 6 \\ 6-3\sqrt{1-\left(\dfrac{6-s}{3}\right)^2} & ; 6 \geq s \geq 3 \\ 6 & ; s < 3 \end{cases} \qquad (20)$$

Note that in this work, the effect of geometry on the plasma edge stability has similar form with that used in Ref. [3], but is somewhat stronger. The function in Eq. (20) can be understood as the following: for *s* > 6, the equation indicates that the pedestal is in the first stability regime of ballooning modes; for 6 ≥ *s* ≥ 3, the equation represents the regime of a transition from first to second stability of ballooning modes; for *s* < 3, the equation represents a plasma that is in the second stability of ballooning modes, where the pedestal pressure gradient is limited by finite *n* ballooning mode stability. It is also noted that the effect of the current-driven peeling mode is not considered in this work. In Eq. (20), the bootstrap current and separatrix effects are included through the calculation of magnetic shear as described in Ref. [3]. Note that magnetic shear in Ref. [3] is calculated as :

$$s = s_0\left(1-\frac{c_{bs}b(\upsilon^*,\varepsilon)\alpha_c}{4\sqrt{\varepsilon}}\right) \qquad (21)$$

where the multiplier c_{bs} indicates the uncertainty of the bootstrap current effect.

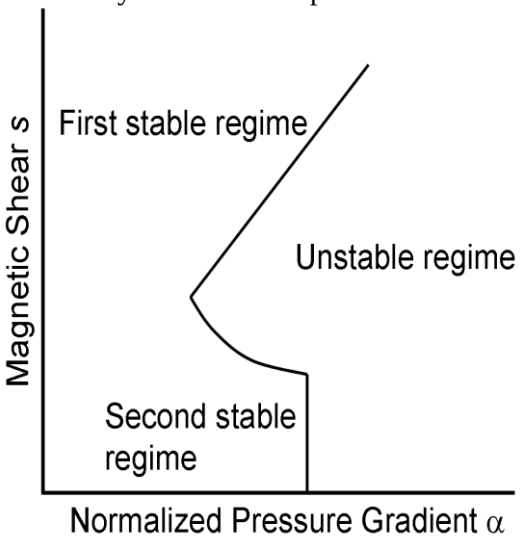

Figure 2: The normalized pressure gradient vs. magnetic shear diagram (s-α diagram) is plotted. First and second stability region and unstable region is also indicated.

3. Experimental Data

The experimental data used in this study are taken from the International Tokamak Physics Activity (ITPA) Pedestal Database [15]. The ITPA Pedestal Database currently contains data from various tokamaks such as the Alcator C-Mod tokamak (C-Mod), the Axially Symmetric Divertor Experiment (ASDEX-U), the

Doublet III-D Tokamak (DIII-D), the Joint European Torus tokamak (JET), and the upgraded Japan Atomic Energy Research Institute Tokamak-60 (JT-60U). In this study, we use data from the current public version of the ITPA Pedestal Database version 3.1, for type 1 ELMy H-mode discharges. As a result, 457 data points from JT-60U and JET are used in this study. In Fig. 3, the experimental data for ion pedestal temperature and the ratio of the electron pedestal density to the Greenwald density are plotted. It can be seen that the ion pedestal temperature decreases, as the ratio of the electron pedestal density to the Greenwald density increases. It is worth noting that the experimental data from JET tends to be in a higher density regime than that for JT-60U.

Statistical comparisons between predicted pedestal parameters and corresponding experimental values obtained from the ITPA Pedestal Database are carried out. To quantify the comparison between the predictions of each model and experimental data, the Root Mean-Square Error (RMSE), the Offset, and the Pearson product moment correlation coefficient (R) are computed. The RMSE, Offset, and correlation R are defined as :

$$\mathrm{RMSE}(\%) = 100 \times \sqrt{\frac{1}{N}\sum_{j=1}^{N}\left[\ln\left(T_j^{\exp}\right) - \ln\left(T_j^{\mathrm{mod}}\right)\right]^2} \tag{22}$$

$$\mathrm{Offset}(\%) = \frac{100}{N}\sum_{j=1}^{N}\left[\ln\left(T_j^{\exp}\right) - \ln\left(T_j^{\mathrm{mod}}\right)\right] \tag{23}$$

$$R = \frac{\sum_{j=1}^{N}\left(\ln\left(T_j^{\exp}\right) - \overline{\ln\left(T_j^{\exp}\right)}\right)\left(\ln\left(T_j^{\mathrm{mod}}\right) - \overline{\ln\left(T_j^{\mathrm{mod}}\right)}\right)}{\sqrt{\sum_{j=1}^{N}\left(\ln\left(T_j^{\exp}\right) - \overline{\ln\left(T_j^{\exp}\right)}\right)^2\left(\ln\left(T_j^{\mathrm{mod}}\right) - \overline{\ln\left(T_j^{\mathrm{mod}}\right)}\right)^2}} \tag{24}$$

where N is total number of data points, and $T_j^{\exp}$ and T_j^{mod} are the j^{th} experimental and model results for the temperature.

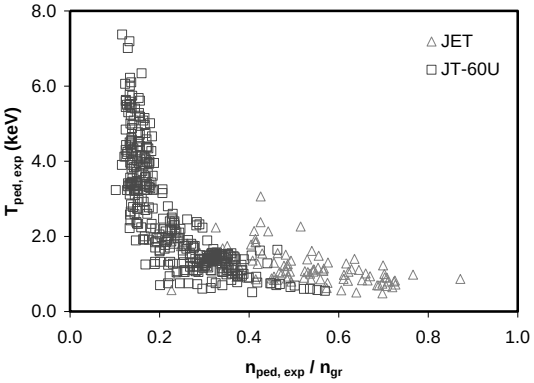

Figure 3: Experiment ion pedestal temperature is plotted against the corresponding experimental electron pedestal density.

4. Results and Discussions

The comparisons between the predictions of the pedestal models developed are compared against experimental data obtained from the ITPA Pedestal Database version 3.2.

4.1 *H*-mode Pedestal Temperature Models

Six scalings for the pedestal temperature are derived using the six models described above for the width of the pedestal together with the model for the critical pressure gradient that includes both first and second stability of ballooning modes. The pedestal temperature scalings are calibrated using 457 experimental data points (90 from JET experiment, and 367 from JT-60U experiment) for the ion pedestal temperature from the ITPA Pedestal Database. The comparisons between the predictions of the models and experimental data are shown in Figs. 4-9. The statistical results are shown in Table 2 for the RMSEs (the fourth column), the correlation R (the fifth column) and the Offset (the sixth column). The value of the coefficient, C_{w}, used in each of the expressions for the pedestal width and the value of multiplier C_{bs} used in the calculation of magnetic shear are given in the second and third column of Table 2,

respectively. It is found that the RMSEs for the pedestal temperature range from 28.2% to 109.4%, where the model based on $\Delta \propto \rho s^2$ yields the lowest RMSE. For the offset, it is shown in Table 1 that the Offsets range from -6.5% to 9.0%, where the model based on $\Delta \propto \rho s^2$ yields the best agreement. For the correlation *R*, it is shown in Table 1 that the values of correlation *R* range from 0.28 to 0.80, where the model based on $\Delta \propto \rho s^2$ yields the best agreement. From these results, it can be concluded that the pedestal temperature model based on $\Delta \propto \rho s^2$ yields the best agreement with experimental data. In Ref.[3], the agreement of the pedestal temperature based on $\Delta \propto \rho s^2$ together with the first ballooning mode pressure gradient model was found to be 32%, which is higher than that found in this paper.

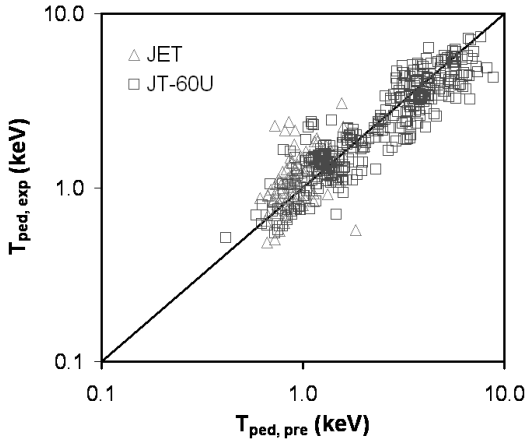

Figure 4: Experimental ion pedestal temperature for type I H-mode plasmas compared with the model predictions based on magnetic and flow shear stabilization width scaling.

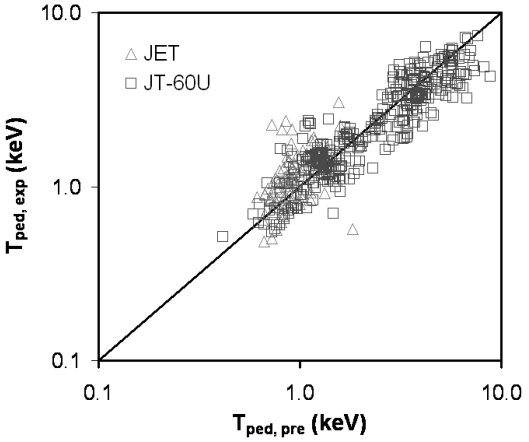

Figure 5: Experimental ion pedestal temperature for type I H-mode plasmas compared with the model predictions based on flow shear stabilization width scaling.

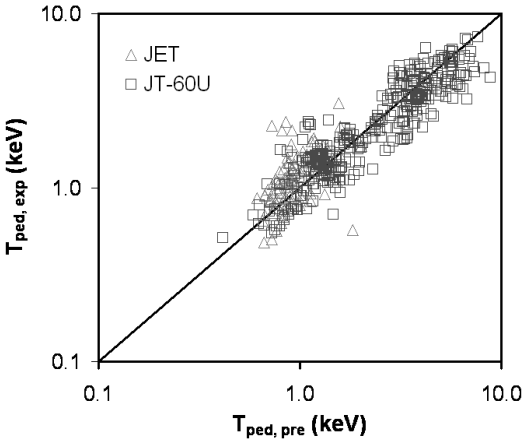

Figure 6: Experimental ion pedestal temperature for type I H-mode plasmas compared with the model predictions based on normalized poloidal pressure width scaling.

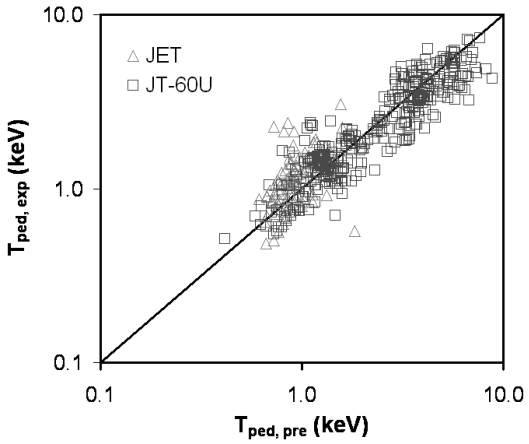

Figure 7: Experimental ion pedestal temperature for type I H-mode plasmas compared with the model predictions based on 2D fluid equilibria width scaling.

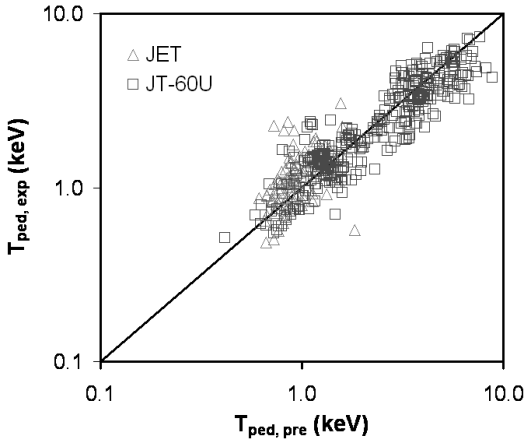

Figure 8: Experimental ion pedestal temperature for type I H-mode plasmas compared with the model predictions based on diamagnetic stabilization width scaling.

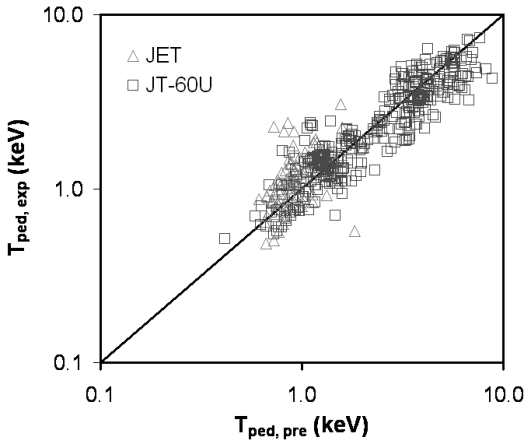

Figure 9: Experimental ion pedestal temperature for type I H-mode plasmas compared with the model predictions based on ion orbit loss width scaling.

Table 1: Notation used in this paper

Symbol	Unit	Description
a	m	Plasma minor radius (half-width)
r	m	Flux surface minor radius (half-width)
R	m	Major radius to geometric center of each flux surface
κ		Plasma elongation
δ		Plasma triangularity
B_T	Tesla	Vacuum toroidal magnetic field at R
I_p	MA	Toroidal plasma current
Mi	AMU	Hydrogenic mass
n_e	m^{-3}	Electron density
T_e	keV	Electron temperature
T_i	keV	Ion temperature
β		Beta $[k(n_eT_e+n_iT_i)/(B_T{}^2/2\mu_o)]$
ρ	m	Ion gyroradius
s		Magnetic shear
q		Safety factor

Table 2: Statistical results of the models for type I ELMy *H*-mode discharges.

Pedestal width scaling	C_w	C_{bs}	RMSE (%)	Offset (%)	R
$\Delta \propto \rho s^2$	5.10	3.0	28.2	0.5	0.80
$\Delta \propto (\rho Rq)^{1/2}$	0.22	4.5	35.4	2.9	0.75
$\Delta \propto R(\beta_{\theta,ped})^{1/2}$	1.50	3.7	35.5	-1.0	0.73
$\Delta \propto (1/Z)$ $(A_H/n_{ped})^{1/2}$	0.60	5.9	50.5	-6.5	0.68
$\Delta \propto \rho^{2/3} R^{1/3}$	1.37	4.9	49.3	-1.1	0.67
$\Delta \propto \varepsilon^{1/2} \rho_\theta$	2.75	4.9	109.4	9.0	0.28

4.2 *H*-Mode Pedestal Density Models

In the development of the pedestal density model, an empirical approach is employed. For the simplest scaling, the pedestal density is assumed to be a function of line average density (n_l). This assumption is based on an observation that the density profile between the pedestal and the magnetic axis in *H*-mode discharges is usually rather flat. Therefore, the pedestal density is a large fraction of the line average density. It is found that the pedestal density scaling for type I ELMy *H*-mode discharges is about 72% of the line average density, which can be described as :

$$\boldsymbol{n_{ped}} = 0.72\boldsymbol{n_l} \qquad (25)$$

This scaling yields an RMSE of 12.2%, R of 0.98, and offset of -2.2% with a data set of 626 data points (132 from ASDEX-U experiment, 127 from JET experiment, and 367 from JT-60U experiment). This scaling is almost the same with the model shown in Ref. [16]. In Ref. [16], a pedestal density scaling is developed for Alcator C-MOD *H*-mode discharges. This scaling is expressed as a function of the line average density, plasma current (I_p), and toroidal magnetic field (B_T). Using this kind of power law regression fit for the 626 data points in the ITPA Pedestal Database (Version 3.2), the best predictive pedestal density scaling for type I ELMy *H*-mode discharges is found to be :

$$\boldsymbol{n_{ped,20}} = 0.74\boldsymbol{n_{l,20}^{0.99}} \boldsymbol{I_p^{0.15}} \boldsymbol{B_T^{-0.12}} \qquad (26)$$

This scaling yields an RMSE of 10.9%, R of 0.98, and offset of 3.3%. The comparisons of the density models' predictions for the pedestal density using Eqs. (25) and (26) and the experimental data are shown in Figs. 10 and 11, respectively. In both figures, the agreement is good for a low ratio of pedestal density to the Greenwald density. However, the agreement tends to break away at high density. This indicates that the physics that controls low and high edge density might be different.

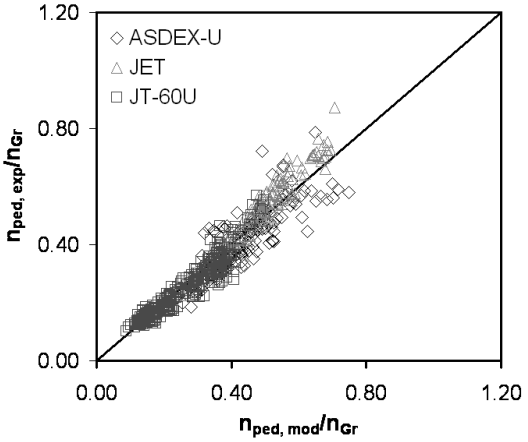

Figure 10: The ratios of experimental pedestal electron density for type I H-mode plasmas to the Greenwald density, are compared with the ratio of the model predictions, using Eq. (25) to the Greenwald density.

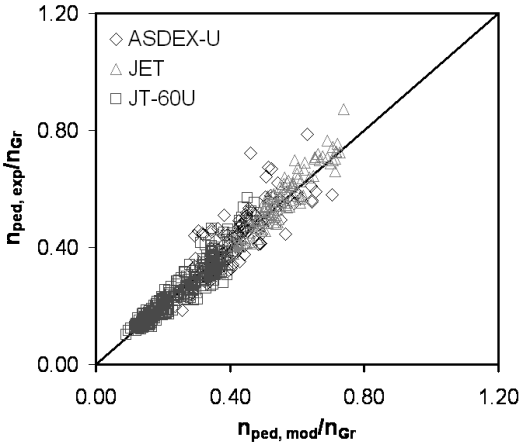

Figure 11: The ratios of experimental pedestal electron density for type I H-mode plasmas to the Greenwald density, are compared with the ratio of the model predictions, using Eq. (26) to the Greenwald density.

4.3 Pedestal Predictions in ITER

The pedestal temperature and density models developed in this paper are used to predict the pedestal parameters for the ITER design. For an ITER standard *H*-mode discharge with 15 MA plasma current and the line average density of 1.05×10^{20} particles/m^3, the pedestal density is predicted to be 0.76×10^{20} particles/m^3 and 0.95×10^{20} particles/m^3 using Eqs. (25) and (26), respectively. It is worth noting that the pedestal density using Eq. (26) indicates a flat density profile since the pedestal density is almost the same as the line average density. This observation is often observed in *H*-mode experiments with high density. In addition, the pedestal density in ITER predicted using an integrated modeling code JETTO yields similar result for the density profile [17]. The pedestal temperature model based on the width of the pedestal as $\Delta \propto \rho s^2$ and the critical pressure gradient model, that includes both first and second stability of ballooning modes, is used to predict the pedestal temperature in ITER. Figure 12 shows the predicted pedestal temperature as a function of pedestal density. It can be seen that the pedestal temperature decreases as the pedestal density increases. At the predicted pedestal density using Eqs. (25) and (26), the predicted pedestal temperature is 1.9 and 1.7, respectively. Under these conditions, it is found that the pedestal width in ITER predicted by the model ranges from 4 to 5 cm.

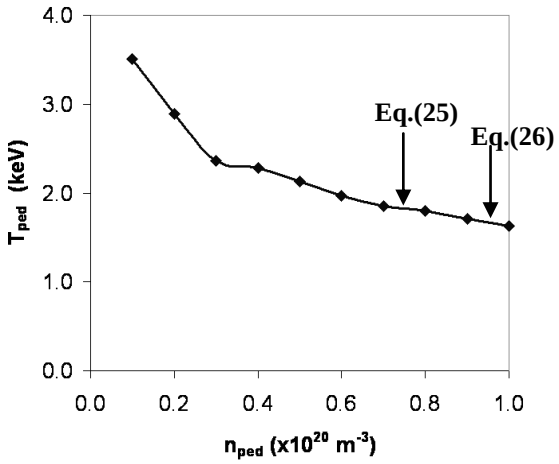

Figure 12: Predictions of pedestal temperature as a function of pedestal density using the pedestal temperature model based on magnetic and flow shear stabilization width scaling.

5. Conclusions

Models for predicting pedestal ion temperature and pedestal electron density at the edge of type I ELMy *H*-mode plasmas are developed. Pedestal ion temperature models include the effects of both the first and second stability of ballooning modes. The results for the pedestal ion temperature are compared with experimental data obtained from the ITPA Pedestal Database version 3.2. It is found that the inclusion of second ballooning stability effect can improve the predictive capability. The pedestal temperature model based on the magnetic and flow shear stabilization yields the best agreement with experimental data

(RMSE of 28.2%). The pedestal density is developed using an empirical approach. It is found that the best model yields an agreement of 10.9% RMSE when its predictions are compared against experimental data. Both pedestal tempera-ture and density models are used to predict the pedestal parameters for the standard type I ELMy *H*-mode scenario of ITER, predictive analysis yields the pedestal ion temperatures in the range from 1.7 to 1.9 keV.

6. Acknowledgements

T. Onjun is grateful to Dr. Glenn Bateman, Prof. Dr. Arnold H. Kritz, and Prof. Dr. Suthat Yoksan for helpful discussions and also thanks the ITPA Pedestal Database group for the pedestal data used in this work. This work is supported by Commission on Higher Education and the Thailand Research Fund (TRF) under Contract No. MRG4880165.

7. References

[1] Kinsey, J.E., Bateman, G., Onjun, T., *et al.*, Burning Plasma Projections Using Drift-Wave Transport Models and Scalings for the *H*-mode Pedestal, Nucl. Fusion, Vol. 43, pp. 1845, 2003.

[2] Aymar, R., Barabaschi, P. and Shimomura, Y. (for the ITER team), The ITER Design, Plasma Phys. Control. Fusion, Vol. 44, pp. 519, 2002.

[3] Onjun, T., Bateman, G., Kritz, A.H., *et al.*, Models for the Pedestal Temperature at the Edge of *H*-mode Tokamak Plasmas, Physics of Plasmas, Vol. 9, pp. 5018. 2002.

[4] Sugihara, M., Igitkhanov, Yu., Janeschitz, G., *et al.*, A Model for *H*-mode Pedestal Width Scaling Using the International Pedestal Database, Nuclear Fusion, Vol. 40, pp. 1743, 2000.

[5] Osborne, T.H., Burrell, K.H., Groebner, R.J., *et al.*, *H*-mode Pedestal Characteristics in ITER Shape Discharges on DIII-D, Journal of Nuclear Materials, Vol. 266-269, pp. 131, 1999.

[6] Guzdar P. N., Mahajan, S. M., and Yoshida, Z., A Theory for the Pressure Pedestal in High (H) Mode Tokamak Discharges**,** Physics of Plasmas, Vol. 12, 032502, 2005.

[7] Shaing, K. C., Poloidal Magnetic Field Dependence of the Edge Electric Field Layer Width in the *H*-mode in Tokamaks, Phys. Fluids B, Vol. 4, pp. 290, 1992.

[8] Rogers, B. N., and Drake, J. F., Diamagnetic Stabilization of Ideal Ballooning Modes in the Edge Pedestal, Phys. Plasmas, Vol.6, pp.2797, 1999.

[9] Kamada, Y., Hatae, T., Fukuda, T., *et al.*, Growth of the Edge Pedestal in JT-60U ELMy *H*-mode, Plasma Phys. Control. Fusion, Vol. 41, pp. 1371, 1999.

[10] Osborne, T.H., Ferron, J.R., Groebner, R.J., *et al.*, The Effect of Plasma Shape on *H*-mode Pedestal Characteristics on DIII-D, Plasma Phys. Control. Fusion, Vol. 42, pp. A175, 2000.

[11] Suttrop, W., Gruber, O., Kurzan, B., *et al.*, Effect of Plasma Shape Variation on ELMs and *H*-mode Pedestal Properties in ASDEX Upgrade, Plasma Phys. Control. Fusion, Vol. 42, pp. A97, 2000.

[12] Wesson, J., Tokamaks, Clarendon Oxford England, 1997.

[13] Stotler, D. P., Reiersen, W. T., and Bateman, G., ASPECT: An Advanced Specified-Profile Evaluation Code for Tokamaks, Comput. Phys. Commun., Vol 81, pp. 261, 1994.

[14] Onjun, T., Kritz, A.H., Bateman, G., *et al.*, Integrated Pedestal and Core Modeling of Joint European Torus

(JET) Triangularity Scan Discharges, Phys. Plasmas, Vol. 11, pp. 3006, 2004.

[15] Hatae, T., Sugihara, M., Hubbard, A.E., *et al.*, Understanding of *H*-mode Pedestal Characteristics Using the Multimachine Pedestal Database, Nucl. Fusion, Vol. 41, pp. 285, 2001.

[16] Bateman, G., Onjun, T., and, Kritz, A.H., Integrated Predictive Modelling Simulations of Burning Plasma Experiment Designs, Plasma Phys. Control. Fusion,Vol. 45, pp. 1939, 2003.

[17] Hughes, J. W., Mossessian, D. A., Hubbard, A. E., *et a*l., Observations and Empirical Scalings of the High-Confinement Mode Pedestal on Alcator C-Mod, Physics of Plasmas, Vol. 9, pp. 3019, 2002.

[18] Onjun, T., Bateman, G., Kritz, A.H., *et al.* Magnetohydrodynamic-Calibrated Edge-localized Mode Model in Simulations of International Thermonuclear Experimental Reactor, Physics of Plasmas, Vol. 12, pp. 082513, 2005.